COMMUNICATION

Coupling the Chemical Reactivity of Bimetallic Surfaces to the **Orientations of Liquid Crystals**

Received 00th January 20xx. Accepted 00th January 20xx

DOI: 10.1039/x0xx00000x

Tibor Szilvási ^{o,#}, Huaizhe Yu ^{b,#}, Jake I. Gold^a, Nanqi Bao^b, Trenton J. Wolter^a, Robert J. Twieg^c, Nicholas L. Abbott^{b,*}, and Manos Mavrikakis^{a,*}

The development of responsive soft materials with tailored functional properties based on the chemical reactivity of atomically precise inorganic interfaces has not been widely explored. In this communication, guided by first-principles calculations, we design bimetallic surfaces comprised of atomically thin Pd layers deposited onto Au that anchor nematic liquid crystalline phases of 4'-n-pentyl-4-biphenylcarbonitrile (5CB), and demonstrate that the chemical reactivity of these alloy surfaces towards Cl2 gas can be tuned by specification of the composition of the surface alloy. Specifically, we use underpotential deposition to prepare submonolayer to multilayers of Pd on Au and employ X-ray photoelectron and infrared spectroscopy to validate computational predictions that binding of 5CB depends strongly on the Pd coverage, with ~0.1 monolayer (ML) of Pd sufficient to cause the liquid crystal (LC) to adopt a perpendicular binding mode. Computed heats of dissociative adsorption of Cl2 on PdAu alloy surfaces predict displacement of 5CB from these surfaces, a result that is also confirmed by experiments revealing that 1 ppm Cl₂ triggers orientational transitions of 5CB. By decreasing the coverage of Pd on Au from 1.8±0.2 ML to 0.09±0.02 ML, the dynamic response of 5CB to 1 ppm Cl₂ is accelerated 3X. Overall, these results demonstrate the promise of hybrid responsive materials designs based on atomically precise interfaces formed between hard bimetallic surfaces and soft matter.

Introduction

with desired functions is to understand how atomic-level structure and composition of interfaces impact functional

A key challenge underlying the design of responsive materials

Electronic Supplementary Information (ESI) available: [details of any supplementary information available should be included here]. See DOI: 10.1039/x0xx00000x

properties.1-5 Liquid crystals (LCs), which combine key properties of crystalline solids (long-range order) and of isotropic liquids (molecular mobility), are a promising class of chemoresponsive materials because the orientations of molecules (mesogens) within LCs, termed the director, can be controlled by the interaction between mesogens and functionalized surfaces. For example, LCs adsorbed on metal salt surfaces can be displaced by preferential adsorption of organophosphates, triggering orientational transitions of the supported LCs.7 Analogously, orientational transition of LCs can be triggered by surface redox reactions that modulate the binding strength of mesogens to surfaces decorated with metal cations.8 However, these past studies have focused on functional surfaces comprising metal salts that can reorganize upon contact with LCs and thus are difficult to manipulate precisely.

In contrast, studies in the field of heterogeneous catalysis, where adsorption, reaction, and desorption are key elementary processes, has led to a range of metal nanostructures with tunable chemical reactivity.9-13 That understanding serves as a fertile source of inspiration for design of LC systems that amplify surface reactions into macroscopic scale optical changes. In particular, a recent study shows that dehydrogenation of aromatic carboxylic acids doped into nematic films of 4'-npentyl-4-biphenylcarbonitrile (5CB) induce 5CB to adopt a perpendicular (homeotropic) orientation on Au(111) and that subsequent dissociative adsorption of Cl₂ on the Au surface can trigger an orientational transition of the LC.14 In this paper, we build from this past study to describe the design of reactive metal alloy surfaces that, via atomic level control of their structure and composition, make possible tuning of the chemical responsiveness of LCs without use of dopants. 15-17

describe a first-principles-guided chemoresponsive LCs by tailoring the composition and reactivity of bimetallic surfaces via use of underpotential deposition. By changing the bimetallic surface composition, we modulate the binding strength of mesogens and of specific analytes to these surfaces. We illustrate the approach using Cl2

^{a.} Department of Chemical and Biological Engineering, University of Wisconsin–Madison, 1415 Engineering Drive, Madison, Wisconsin 53706, United

^{b.} Robert Frederick Smith School of Chemical and Biomolecular Engineering, Cornell University, 1 Ho Plaza, Ithaca, New York 14853, United States.

^{c.} Department of Chemistry and Biochemistry, Kent State University, 1175 Risman Drive, Kent, Ohio 44242, United States

[#] T.S. and H. Y. contributed equally to this work.

^{*} Email: nabbott@cornell.edu and emavrikakis@wisc.edu

COMMUNICATION Journal Name

as the analyte and its dissociative adsorption on bimetallic PdAu surfaces as the driver of the LC orientational transition. More broadly, our work demonstrates how insights from fundamental surface science and catalysis of bimetallics can

lead to innovative atomic-scale designs of chemoresponsive LC systems.

Results and Discussion

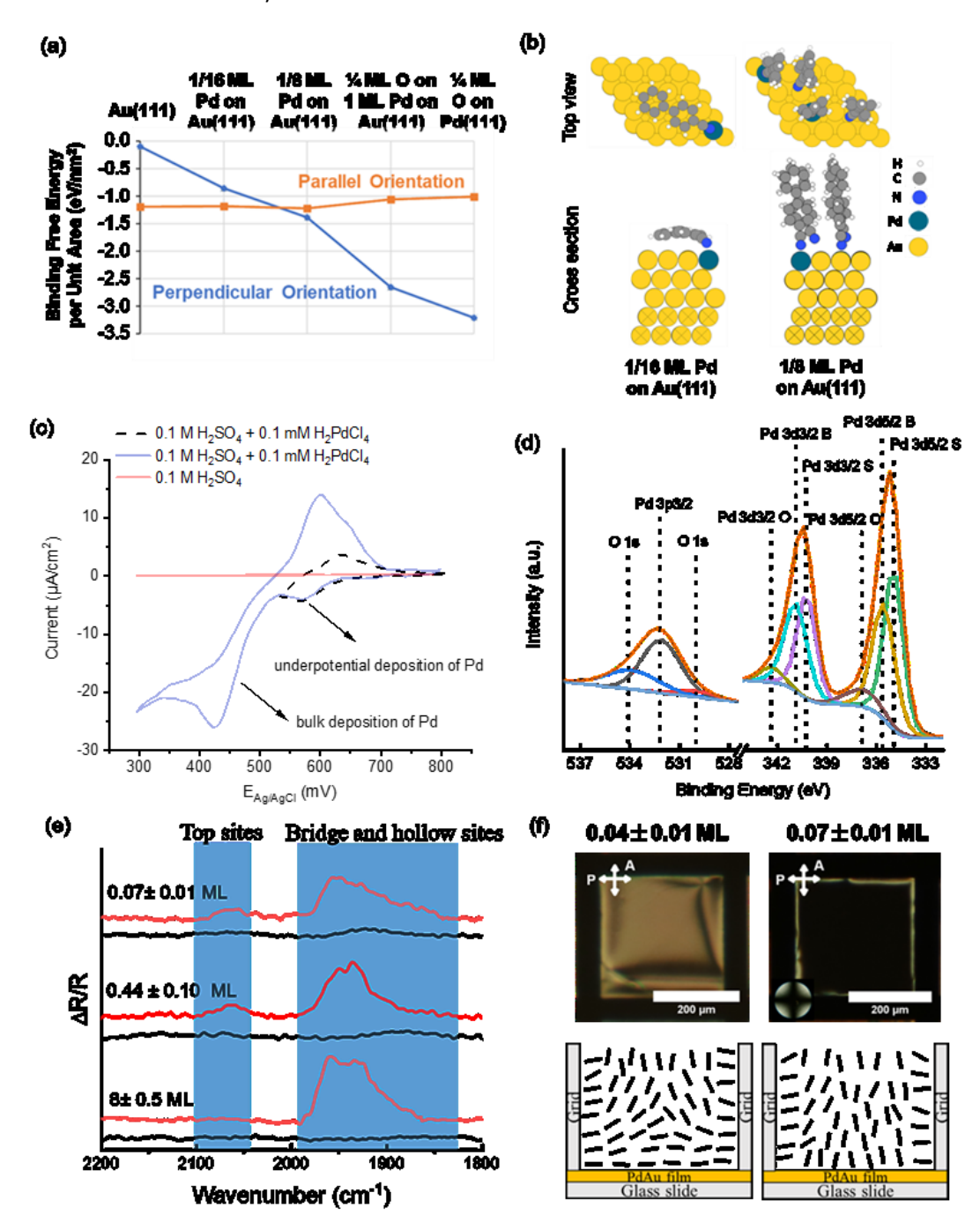


Figure 1. (a) Calculated Binding Free Energy per unit Area (BFE/A) of PhPhCN in parallel and perpendicular adsorption orientation for five model surfaces with varying Pd content. (b) The energetically favored parallel (perpendicular) orientation of PhPhCN on 1/16 (1/8) ML Pd on Au(111) in a 4x4 unit cell on the left (right). Crossed atoms represent bulk atoms that were not allowed to relax during energy minimization. (c) Cyclic voltammograms for Au film in 0.1 M H₂SO₄ + 0.1 mM H₂PdCl₄ with a return at 300 mV (light blue line) and a return at 530 mV (dark dash line), and in 0.1 M H₂SO₄ (red solid line). Scan rate: 5 mV/s. (d) X-ray photoelectron spectroscopy (XPS) showing Pd and O peaks on ~80 ML of Pd/Au surface. B, S, and O indicate bulk Pd, surface Pd, and O covered surface Pd, respectively. (e) Fourier transformed polarization-modulation infrared reflectance absorbance spectroscopy (PM-IRRAS) of different MLs of Pd on Au surface before (black line) and after (red line) exposure to a N₂ stream containing 2% CO for 20 mins. (f) Optical micrographs (crossed polars) of micrometer-thick films of 5CB deposited on gold films with 0.04±0.01 ML of Pd and 0.07±0.01 ML of Pd. A schematic representation of the LCs is shown below each optical image.

Journal Name COMMUNICATION

To understand the orientation of 5CB adsorbed on PdAu alloy surfaces with different Pd content, we performed periodic Density Functional Theory (DFT) calculations. 18,19 We built five surface models, evaluated their stability under ambient conditions, and explored the potential for intermixing Pd with Au to form bulk alloys (for details, see Supplementary Information (SI)). We found that for high Pd coverage (1 ML or above), partial ¼ ML O-coverage is present under ambient conditions (see below for experimental evidence). Additional studies are needed to exclude the presence of atomic O on surfaces with less than 1ML Pd in the Au surface. For the purposes of the present study, however, we assumed that there was no oxygen adsorbed on sub-monolayer-Pd Au surfaces. In addition, we showed by computation that all Pd atoms remain on the surface when mesogens are adsorbed on the surface, due to the stronger interaction between mesogen and Pd than mesogen and Au. Based on these results, the five models that we studied ranged from 0 to several MLs of Pd on Au(111): 1/4 ML O-precovered Pd(111), 1 ML Pd on Au(111) with the Pd ML pre-covered by ¼ ML O, 1/8 ML Pd in Au(111), 1/16 ML Pd in Au(111), and Au(111) (for details see the SI). In Figure 1a, we show the calculated binding free energy per unit area (BFE/A), a descriptor that we use to compare the preferred binding modes of adsorbates in different coverages and unit cells (see details in the SI). We used PhPhCN as a surrogate for 5CB for reasons detailed in the SI. We find that the binding of PhPhCN in a parallel orientation depends only modestly on the Pd content of the surface, with BFE/A ranging between -1.0 to -1.2 eV/nm². On the other hand, the binding of PhPhCN in the perpendicular orientation changes substantially with increasing Pd content, with the BFE/A ranging from -0.10 eV/nm² for clean Au(111) to -3.21 eV/nm² for ¼ ML O-precovered Pd(111). When the perpendicular orientation is preferred (Figure 1b, right), the nitrile tail of PhPhCN binds to the top site of Pd atoms though dative bonds, an interaction that is sensitive to the amount of Pd present on the surface. In contrast, PhPhCN binds to the surface in the parallel orientation mainly through dispersion interactions (Figure 1b, left) that depend weakly on the atomic composition of the surface. An electron density difference plot (Figure S3) shows that the d_z² orbital of Pd interacts with the lone pair of the nitrogen atom in PhPhCN and a significant charge transfer takes place from the nitrile group to the d_z² orbital of the Pd (additional analysis can be found in the SI).

Figure 1a shows that the energetically preferred orientation of PhPhCN changes with increasing Pd coverage of the Au(111) surface. The parallel orientation is favored in the case of Au(111) and 1/16 ML Pd on Au(111); perpendicular orientation is preferred on ½ ML O-precovered Pd(111), ½ ML O-precovered 1 ML Pd on Au(111), and 1/8 ML Pd on Au(111). These results predict that at a Pd coverage between 1/16 and 1/8 ML, the orientation of the mesogen film will change from a planar to perpendicular orientation and that at higher Pd coverages a clear preference for the perpendicular alignment is predicted. To test these computational predictions, we electrochemically deposited Pd on vacuum-deposited Au films (predominantly Au(111)) from an aqueous solution containing 0.1 M H₂SO₄ + 0.1 mM H₂PdCl₄ (see SI for details). Cyclic voltammetry (CV) was

first performed to confirm that Pd underpotential deposition on the Au film occurred at 575 mV and that Pd bulk deposition started at 530 mV (see Figure 1c), consistent with prior reports.⁷ Past studies using scanning tunneling microscopy and scanning microscopy show that Pd is electron deposited electrochemically on Au(111) without forming bulk Pd-Au alloys, while Pd is found to form alloys with Au when Pd is deposited through vapor deposition in ultra-high vacuum (UHV) studies. 20,21 To confirm the presence of O on Pd covered surfaces exposed to air, we first deposited 80 ML (calculated from the Coulombic charge) of Pd on Au to eliminate the contribution of O on the Au surface in x-ray photoelectron spectra. As shown in Figure 1d, the measured ratio between the O and Pd surface signal was approximately 0.20, consistent with prior reports of O coverage on Pd(111) surfaces in air at room temperature.8 As shown in Figure S4, with a decrease in

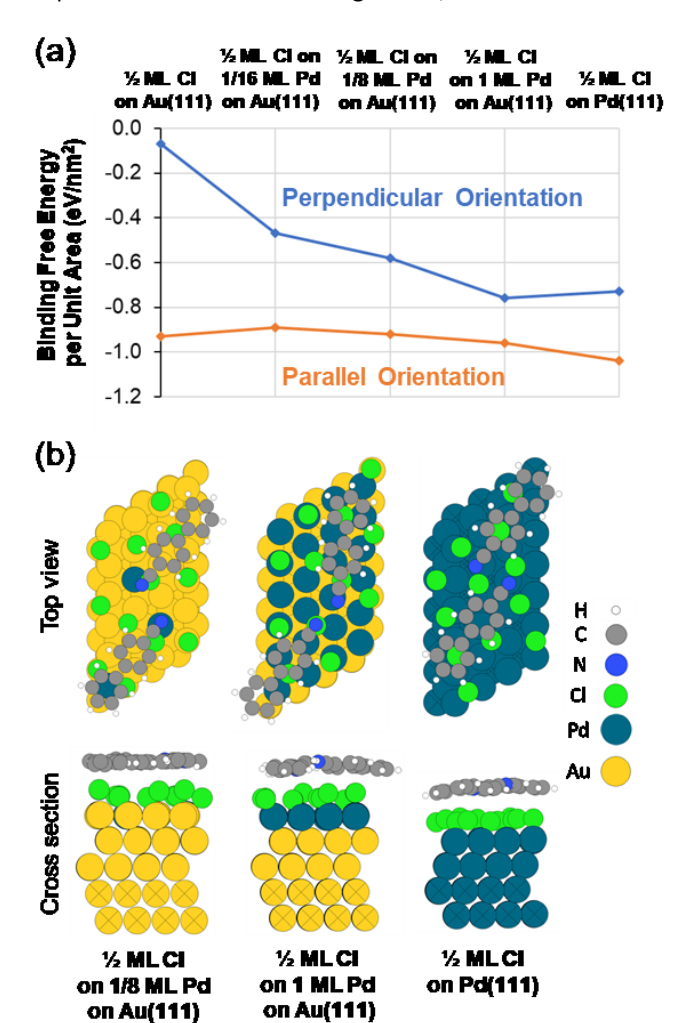


Figure 2. (a) Calculated Binding Free Energy per unit area (BFE/A) of PhPhCN in parallel and perpendicular orientation for five Cl-precovered model surfaces with varying Pd content. (b) Top and side views of the energetically favored parallel orientation of PhPhCN on ½ ML Cl-precovered 1/8 ML Pd on Au(111) (left), on ½ ML Cl-precovered 1 ML Pd on Au(111) (middle), and on ½ ML Cl-precovered Pd(111) (right). These three surfaces preferred perpendicular PhPhCN adsorption in the absence of Cl on the surface.

COMMUNICATION Journal Name

thickness of the Pd deposited onto Au, the Au signal increases while the Pd signal decreases, confirming deposition of Pd on top of the Au. Additionally, the measured binding energies of 340.7 eV for Pd 3d 5/2 and 340.1 eV for Pd 3d 3/2 correspond to pure Pd and indicate the absence of alloy formation. ^{22–24} Infrared spectroscopy performed using CO as a probe molecule (Figure 1e) yielded peaks from 2000 to 1900 cm⁻¹ corresponding

to CO bound at bridge sites of Pd, and indicating that the samples comprising 0.07 ± 0.01 ML and 0.44 ± 0.10 ML Pd on Au present islands of Pd (in contrast, if the Pd was atomically dispersed on the 0.07 ± 0.01 ML sample, the CO would be able to bind only to top sites of the Pd atoms).²⁵

Next, we characterized the orientations of micrometer-thick films of nematic 5CB supported on gold films and Pd containing

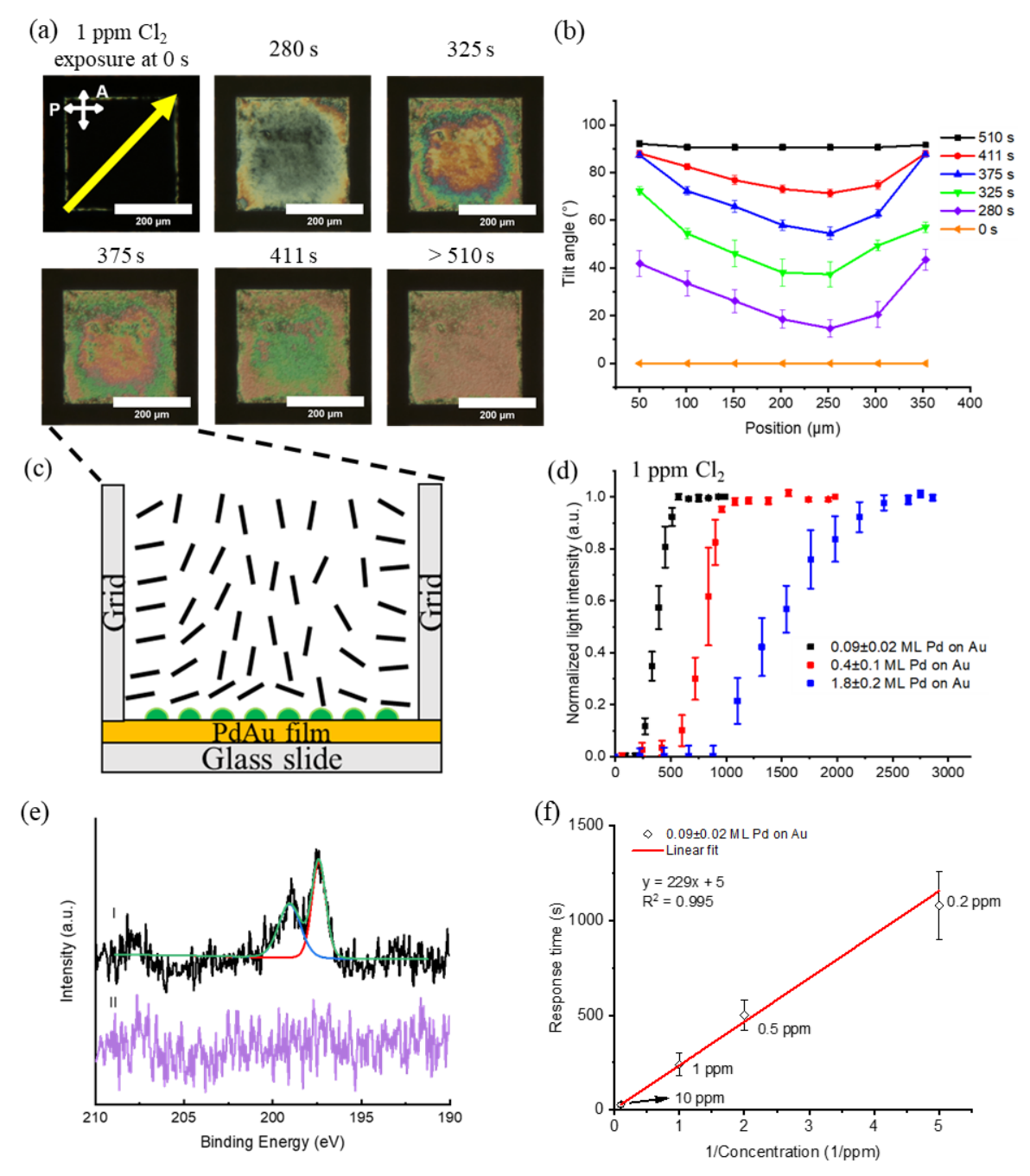


Figure 3. (a) Optical micrographs (crossed polars) of micrometer-thick films of 5CB supported on 0.09±0.02 ML Pd on Au surface exposed to 1 ppm Cl₂. (b) Tilt angles from surface normal for films of 5CB across the diagonal of the square of TEM (along the yellow arrow in (a)). (c) Schematic (cross-sectional view) representation of the LCs of the intermediate state shown in (a). (d) Normalized intensity of polarized light transmitted through 5CB supported on Pd/Au surfaces and then exposed to 1 ppm of Cl₂. (e) XPS showing (I) Cl 2p peaks at 197.4 and 199.0 eV on 8±0.5 ML Pd on Au surface following exposure to Cl₂ gas for 15 mins, and (II) spectrum collected prior to exposure to Cl₂. (f) Linear fitting of the response time of 5CB, supported on 0.09±0.02 ML Pd on Au, to 10, 1, 0.5 and 0.2 ppm Cl₂. The error bar of the point near the origin is smaller than the size of the symbol.

Journal Name COMMUNICATION

Au films using polarized light microscopy (transmission mode). Nematic 5CB exhibited planar anchoring on the Au surface as reported in our previous work¹⁴ while increasing the amount of Pd on Au led to a change in anchoring of the LC. Specifically, we observed the anchoring of 5CB to change from planar (confirmed by the optical colors generated by white-light illumination) to homeotropic (confirmed by conoscopic polarized light microscopy, showing dark cross overlying concentric rings) between 0.04±0.01 ML and 0.07±0.01 ML of Pd on Au (see Figure 1f). This experimental finding is in good agreement with our computational results.

To study the effect of Cl_2 on the interaction of 5CB with AuPd bimetallic surfaces, we first used DFT calculations to predict that Cl_2 dissociatively adsorbs on all five ½ ML PhPhCN covered model surfaces (see detailed discussion in the SI). In addition, we found that ½ ML Cl coverage can form on the model surfaces in the absence of PhPhCN under experimentally relevant conditions (1 ppm Cl_2 at ambient). Accordingly, to describe the surface environments when exposed to Cl_2 , we adopted the following model surfaces: ½ ML Cl-precovered Pd(111), ½ ML Cl-precovered 1 ML Pd on Au(111), ½ ML Cl-precovered 1/8 ML Pd on Au(111), ½ ML Cl-precovered 1/16 ML Pd on Au(111), and ½ ML Cl-precovered Au(111) (details in SI).

Figure 2a shows the calculated BFE/A values for the binding of PhPhCN in parallel and perpendicular orientation on all five ½ ML Cl-precovered model surfaces, revealing that the parallel orientation is favored in all cases. The preferred parallel binding of PhPhCN is shown in Figure 2b for ½ ML Cl-precovered 1/8 ML Pd on Au(111) (left), 1/2 ML Cl-precovered 1 ML Pd on Au(111) (middle), and ½ ML Cl-precovered Pd(111) (right), because these surfaces were predicted and showed experimentally to exhibit a preference for perpendicular PhPhCN orientation before exposure to Cl₂. This change in preferred orientation originates from the destabilization of the perpendicular adsorbed state induced by the presence of coadsorbed Cl. The calculated BFE/A is similar for the parallel adsorbed state before and after introducing ½ ML Cl coverage (see Figure 1a and 2a; values in Table S1), whereas the perpendicular adsorbed state is severely destabilized when coadsorbed with ½ ML Cl. Figure 2b shows that when ½ ML Cl is adsorbed, no Pd atoms are free of CI atoms and thus able to promote the perpendicular adsorption of PhPhCN. An electron density difference plot (see Figure S3) provides additional evidence for the destabilization perpendicular orientation. Figure S3 shows that perpendicular adsorption of PhPhCN on $\frac{1}{2}$ ML Cl-precovered Pd(111) results in smaller charge transfer from the nitrile group to the Pd than the perpendicular adsorption of PhPhCN on 1/4 ML O-precovered Pd(111), which explains the weaker perpendicular binding of PhPhCN on Cl-covered surfaces and the change to preferred planar orientation. Overall, our calculations predicted that exposure of the PdAu surfaces used in our study to Cl₂ can lead to a significant Cl-coverage, capable of disrupting the interaction of the nitrile group with the surface, potentially leading to an observable optical transition in a supported LC.

To test the computational predictions, micrometer-thick films of nematic 5CB were deposited onto PdAu surfaces and

subsequently exposed to a stream of N₂ containing 1 ppm Cl₂ at 1000 mL/min. As shown in Figure 3a, when supported on a 0.09±0.02 ML Pd on Au and exposed to a nitrogen stream containing 1 ppm of Cl₂, 5CB transitioned from the initial dark to a final pale pink optical appearance. The changes in optical interference colors generated using white-light illumination were converted to LC tilted angles (see Figure 3b, see details in the section of Experimental Details in SI), revealing a continuous change of the orientation of 5CB upon exposure to Cl₂. Additionally, the orientational transition was evident first in the region of LC close to the surface of the metallic grid that was used to stabilize the micrometer-thick LC film. This observation is consistent with an orientational response of the LC that elastically strains the LC: LC with a parallel orientation near the vertical surface of the metallic grid minimizes the elastic energy required to initiate the LC response (see Figure 3c and details in SI).²⁶ Subsequent exposure of the samples to N₂ for 1 hour did not result in a change in orientation of 5CB. The irreversible optical response of 5CB to Cl adsorption supports our conclusion of strong binding of CI to the PdAu surface.

Figure 3d shows that 5CB exhibited a faster anchoring transition on the 0.09±0.02 ML Pd/Au than on the 0.4±0.1 ML Pd/Au surface. We hypothesized that these dynamics arise because Cl₂ has to displace more 5CB molecules bound to Pd atoms through dative bonds, when more Pd atoms are available in the surface. To test the hypothesis of Pd coverage-dependent response time, we increased the thickness of Pd deposited on Au to 1.8±0.2 ML. Figure 3d shows that in this case, 5CB exhibited a slower anchoring transition than when it was supported on 0.4±0.1 ML Pd/Au. Finally, to confirm the existence of adsorbed CI on the PdAu surfaces, after exposure to Cl₂ gas, we performed X-ray photoelectron spectroscopy (XPS) measurements both before and after exposure. The 8±0.5 ML Pd/Au films were coated with micrometer-thick films of 5CB, exposed to Cl₂, and then rinsed with ethanol to remove the LC prior to performing XPS. After exposure, two peaks corresponding to Cl 2p at 197.7 and 199.0 eV appears (Figure 3e-I). In contrast, that peak was not present prior to exposure to Cl₂ gas (Figure 3e-II).

By using 0.09 \pm 0.02 ML of Pd on Au to support 5CB, we determined that the response time (5% of the normalized light intensity) changes linearly with the inverse of the Cl₂ concentration (Figure 3f). To provide insight into this observation, as detailed in the SI and elsewhere, 27,28 we developed a simple transport model that describes the characteristic LC response time as

$$t_{total} = \frac{S_{Pd}\theta_{th}}{2K_G C_{B,N2}} + t_{en} + \frac{\delta_{N2}^2}{2D_{N2}} + \frac{\delta_{LC}^2}{2D_{LC}}$$
 (1)

where S_{Pd} is the surface density of Pd (estimated from a DFT derived lattice constant for Pd), θ_{th} is the threshold Cl-coverage on Pd to trigger optical response of LC, K_G is the overall mass transfer coefficient, $C_{B,N2}$ is the concentration of Cl_2 in the bulk, and t_{en} is the time needed for Cl_2 to travel from the gas cylinder to the LC cell. K_G is defined as

to the LC cell.
$$K_G$$
 is defined as
$$K_G = 1/(\frac{\delta_{N2}}{D_{N2}} + \frac{H\delta_{LC}}{D_{LC}}) \tag{2}$$

COMMUNICATION Journal Name

where δ_{N2} is the thickness of vapor phase boundary layer, δ_{LC} is the thickness of LC layer, D_{N2} is the diffusion coefficient of Cl_2 in N_2 , D_{LC} is diffusion coefficient of Cl_2 in the LC phase, and H is the partition coefficient defined as a unit-less ratio of the concentration (mol/volume) of Cl_2 in the air phase divided by the concentration of Cl_2 in liquid crystal phase at equilibrium.

Equation 1 captures the linear relationship between response time and the inverse of Cl_2 concentration indicating that the response of the LC film is diffusion limited. From Eq. 1 and the slope of the line shown in Figure 3f, we conclude that θ_{th} is ~0.25. Additionally, the intercept of the line through the y axis is ~5s, which is similar in magnitude to the last three terms (2.6 s) of Equation 1. In Equation 2, $\delta_{\text{N2}}/D_{\text{N2}} = 2$ s/cm is two orders of magnitude smaller than $H\delta_{\text{LC}}/D_{\text{LC}} = 369$ s/cm, indicating that the dynamic of response of LC film is dominated by mass transport of Cl_2 from the gas-5CB interface to 5CB-PdAu interface (see further discussion in SI).

Additional experiments revealed that the response time of 5CB with a 20 μ m thick LC film is 4, 8, and 16 mins for 1, 0.5, 0.2 ppm Cl₂, respectively. For context, we mention that the US Occupational Safety and Health Administration (OSHA) specifies a short-term exposure limit for workers of 15 minutes for 1 ppm Cl₂, and an 8-hour exposure limit (time-weighted average) of 500 ppb Cl₂. We also found the chemical selectivity of this system to be promising, with no measurable optical response to N₂, 80% relative humidity in N₂ (Figure S9), 10 ppm of DMMP, NO₂, ethylene oxide, or formaldehyde for exposure times of 1 hour. Overall, the approach developed in this paper provides principles for the design of small, passive and lightweight devices that consume no power and can be worn by individuals to monitor personal exposure to Cl₂.

Conclusions

In summary, we have designed a selective chemoresponsive LC system using bimetallic PdAu surfaces and demonstrated that the response of the system can be tailored by using electrochemical deposition to control the Pd content of the surface. The LC response at the bimetallic PdAu surfaces were predicted by computational chemistry, including the observation that 5CB adopts a homeotropic orientation with as little as 0.09±0.02 ML Pd on the Au surface. We show that the reactivity of the bimetallic surfaces can disrupt the binding of the nitrile group to the Pd, thus leading to an orientational transition of the LC upon exposure to the reactant species. We demonstrated this design principle using the example of dissociative adsorption of Cl₂. We envision that by capitalizing on the rich literature of heterogenous catalysis by bimetallic surfaces, the scientific community will be able to efficiently design improved chemoresponsive LC systems for a wide range of chemical species, starting from first principles. Additionally, the results of our study hint at new chemical principles that might be harnessed in future designs of photonic devices that require controlled switching of LC orientations. 29-31

Acknowledgements

T.S. and H. Y. contributed equally to this work. This work was supported by the National Science Foundation (DMREF grant: DMR-1921696, DMR-1921722, and DMR-1921668) and the Army Research Office (W911NF-19-1-0071 and W911NF-15-1-0568). Additionally, the research used facilities supported by the Cornell MRSEC (DMR-1719875). Part of the computational work conducted by T.S., J.I.G., and M.M. was carried out using computational resources available through the DoD High Performance Computing Modernization Program (US Air Force Research Laboratory DoD Supercomputing Resource Center (AFRL DSRC), the US Army Engineer Research and Development Center (ERDC), and the Navy DoD Supercomputing Resource Center (Navy DSRC), ARONC43623362), supported by the Department of Defense; and the National Energy Research Scientific Computing Center (NERSC) through the U.S. DOE, Office of Science under Contract No. DE-AC02-05CH11231.

Conflicts of interest

NLA declares a financial interest in Platypus Technologies LLC, a for-profit company that has commercialized liquid crystal-based sensors.

Notes and references

- 1 S. M. Mirvakili and I. W. Hunter, Adv. Mater., 2018, 30, 1.
- L. Zhang, P. Naumov, X. Du, Z. Hu, and J. Wang, Adv. Mater., 2017, 29, 1.
- 3 D. G. Montjoy, J. H. Bahng, A. Eskafi, H. Hou, and N. A. Kotov, J. Am. Chem. Soc., 2018, 140, 7835.
- 4 M. E. Prévôt, A. Nemati, T. R. Cull, E. Hegmann, and T. Hegmann, *Adv. Mater. Technol.*, 2020, **5**, 2000058.
- 5 T. Kato, J. Uchida, T. Ichikawa, and T. Sakamoto, *Angew. Chemie Int. Ed.*, 2018, **57**, 4355.
- 6 E. Bukusoglu, M. Bedolla Pantoja, P. C. Mushenheim, X. Wang, and N. L. Abbott, *Annu. Rev. Chem. Biomol. Eng.*, 2016, 7, 163.
- 7 R. R. Shah and N. L. Abbott, *Science*, 2001, **293**, 1296.
- 8 T. Szilvási, N. Bao, K. Nayani, H. Yu, P. Rai, R. J. Twieg, M. Mavrikakis, and N. L. Abbott, Angew. Chemie Int. Ed., 2018, 57, 9665
- W. Y. Yu, L. Zhang, G. M. Mullen, E. J. Evans, G. Henkelman, and C. B. Mullins, *Phys. Chem. Chem. Phys.*, 2015, 17, 20588.
- L. Luo, Z. Duan, H. Li, J. Kim, G. Henkelman, and R. M. Crooks, J. Am. Chem. Soc., 2017, 139, 5538.
- 11 Q. K. Do, H. V. Tran, S. Wang, and L. C. Grabow, *Energy Technol.*, 2020, **8**, 1900732.
- 12 J. L. Johnson, A. Behnam, S. J. Pearton, and A. Ural, Adv. Mater., 2010, 22, 4877.
- 13 Q. Feng, S. Zhao, Q. Xu, W. Chen, S. Tian, Y. Wang, W. Yan, J. Luo, D. Wang, and Y. Li, Adv. Mater., 2019, 31, 1901024.
- 14 H. Yu, T. Szilvási, K. Wang, J. I. Gold, N. Bao, R. J. Twieg, M. Mavrikakis, and N. L. Abbott, J. Am. Chem. Soc., 2019, 141, 16002
- Y. Han, K. Pacheco, C. W. M. Bastiaansen, D. J. Broer, and R. P. Sijbesma, J. Am. Chem. Soc., 2010, 132, 2961.
- 16 S. Tokunaga, Y. Itoh, H. Tanaka, F. Araoka, and T. Aida, J. Am. Chem. Soc., 2018, 140, 10946.
- 17 P. V. Shibaev, O. Roslyak, J. Plumitallo, E. Gullatt, and U. Aparajita, *Appl. Phys. A*, 2020, **126**, 920.

Journal Name COMMUNICATION

- 18 G. Kresse and J. Furthmüller, *Phys. Rev. B*, 1996, **54**, 11169.
- 19 G. Kresse and J. Furthmüller, *Comput. Mater. Sci.*, 1996, **6**, 15.
- L. A. Kibler, M. Kleinert, R. Randler, and D. M. Kolb, Surf. Sci. 1999, 443, 19.
- 21 B. E. Koel, A. Sellidj, and M. T. Paffett, *Phys. Rev. B*, 1992, **46**, 7846.
- 22 D. Zemlyanov, B. Aszalos-Kiss, E. Kleimenov, D. Teschner, S. Zafeiratos, M. Hävecker, A. Knop-Gericke, R. Schlögl, H. Gabasch, W. Unterberger, K. Hayek, and B. Klötzer, Surf. Sci., 2006, 600, 983.
- 23 J. Greeley and M. Mavrikakis, J. Phys. Chem. B, 2005, 109, 3460.
- 24 F. P. Leisenberger, G. Koller, M. Sock, S. Surnev, M. G. Ramsey, F. P. Netzer, B. Klötzer, and K. Hayek, Surf. Sci., 2000, 445, 380.
- 25 G. Rupprechter, T. Dellwig, H. Unterhalt, and H.-J. Freund, J. Phys. Chem. B, 2002, 105, 3797.
- 26 K. Nayani, P. Rai, N. Bao, H. Yu, M. Mavrikakis, R. J. Twieg, and N. L. Abbott, *Adv. Mater.*, 2018, **30**, 1706707.
- 27 J. T. Hunter and N. L. Abbott, Sensors Actuators B Chem., 2013, 183, 71.
- 28 J. K. Sheavly, J. I. Gold, M. Mavrikakis and R. C. Van Lehn, *Mol. Syst. Des. Eng.*, 2020, **5**, 304.
- 29 M. V. Gorkunov, I. V. Kasyanova, V. V. Artemov, A. A. Ezhov, A. V. Mamonova, I. V. Simdyankin, and S. P. Palto, *ACS Photonics*, 2020, **7**, 3096.
- 30 M. V. Gorkunov, I. V. Kasyanova, V. V. Artemov, A. A. Ezhov, A. V. Mamonova, I. V. Simdyankin, and S. P. Palto, ACS Appl. Mater. Interfaces, 2020, 12, 30815.
- 31 I. Nys, Liquid Crystal Today, 2021, 29, 65.